When multilayer links exchange their roles in synchronization

Longkun Tang •, 1,2 Kelley Smith, 2 Kevin Daley •, 2 and Igor Belykh • 2,*

1 School of Mathematical Sciences, Huaqiao University, Quanzhou 362021, China
2 Department of Mathematics and Statistics, Georgia State University, P.O. Box 4110, Atlanta, Georgia 30302-410, USA



(Received 10 January 2022; revised 25 June 2022; accepted 9 August 2022; published 26 August 2022)

Real world networks contain multiple layers of links whose interactions can lead to extraordinary collective dynamics, including synchronization. The fundamental problem of assessing how network topology controls synchronization in multilayer networks remains open due to serious limitations of the existing stability methods. Towards removing this obstacle, we propose an approximation method which significantly enhances the predictive power of the master stability function for stable synchronization in multilayer networks. For a class of saddle-focus oscillators, including Rössler and piecewise linear systems, our method reduces the complex stability analysis to simply solving a set of linear algebraic equations. Using the method, we analytically predict surprising effects due to multilayer coupling. In particular, we prove that two coupling layers—one of which would alone hamper synchronization and the other would foster it—reverse their roles when used in a multilayer network. We also analytically demonstrate that increasing the size of a globally coupled layer, that in isolation would induce stable synchronization, makes the multilayer network unsynchronizable.

DOI: 10.1103/PhysRevE.106.024214

I. INTRODUCTION

Many natural and engineering networks contain units that are coupled through multiple interaction layers [1-3]. Neurons are often coupled via excitatory, inhibitory, and electrical synapses whose co-action may lead to synergistic effects [4,5]. Multilayer networks can exhibit rich cooperative dynamics [1,6–8], including complete synchronization [9-12], clusters of synchrony [13-15], explosive [16], interlayer and intralayer [17,18], and relay synchronization [19]. When compared with their single-layer counterparts, the role of multilayer network topologies in promoting or hampering synchronization is significantly less understood [20-36]. Two hallmark methods, the master stability function [20] and the connection graph method [25,26], are generally used to predict the stability of synchronization in a single-layer network. However, the predictive power of the master stability function [9–11] is severely impaired in multilayer networks. This is due to the fact that the connectivity matrices that represent interaction layers typically cannot be diagonalized simultaneously and thus their eigenvalues are not informative. The most successful application of the master stability function to multilayer networks was performed in Ref. [10]. This approach consists in simultaneous block diagonalization (SBD) of the connectivity matrices [10] that can reduce the dimensionality of the stability problem. However, it remains a limited approach because the results of the reduction can remain difficult to analyze [37]. Reductions typically yield networks with weighted positive and negative connections as well as self-loops.

As an alternative, the connection graph-based method for assessing the impact of multilayer network topology on synchronization was recently developed in Ref. [12]. This method connects the stability of synchronization with traffic loads on critical edges. Its application to multilayer networks revealed a "when good links go bad" effect in which replacing a link by a pairwise stabilizing coupling via another layer can make the network unsynchronizable, turning the "good" link into a destabilizing connection [12]. However, this method is restricted to oscillator networks with an unbounded interval of coupling for which synchronization is stable. Networks of Lorenz oscillators [25] and Hodgkin-Huxley-type neurons [38] are representative examples of such an "unbounded" type of synchronization behavior. There is a critical gap in research methods that can explicitly relate the stability of synchronization to structural changes in multilayer oscillator networks of "bounded" type that remain synchronized only in a bounded region of coupling strength [20]. This important class of networks includes coupled tritrophic Rozenzweig-MacArthur models [39], Duffing oscillators [40], Van der Pol oscillators [41], and x-coupled Rössler systems that are widely used as a test bed [20,22,32,42] for probing the master stability function. Therefore, to date, the synchronization properties of multilayer networks of Rössler and other oscillators of the bounded type remain poorly understood and are typically studied on a case by case basis via full-scale simulations of all Lyapunov exponents of the high-dimensional networked

In this paper, we aim to close this gap by offering an approximation method that can significantly improve the predictive power of the SBD methods [10,15] or any other possible generalization of the master stability function. Our method is based on a structural property of a class of saddle-focus oscillators, including Rössler [43] and piecewise

^{*}ibelykh@gsu.edu

linear saddle-focus systems [44], which indicates that the stabilization of the focal part of the synchronous trajectory determined by a linear system implies the overall stability of synchronization. As a result, our approach reduces the dimensionality of the stability problem and replaces numerical calculations of Lyapunov exponents with a lower-dimensional set of linear algebraic equations amenable to analytical treatments.

The paper is organized as follows: In Sec. II, we introduce the multilayer network model. In Sec. III, we start with the simplest three-node multilayer network of Rössler oscillators with synchronization properties drastically different from its single-layer counterpart. We formulate our approximation method that yields tight bounds for the stability of synchronization and predicts counterintuitive effects caused by multilayer coupling. In Sec. IV, we study networks that allow significant SBD reduction. In Sec. V, we further verify the predictive power of our method for synchronization in multilayer networks with arbitrary topologies. Beyond Rössler oscillators, in Sec. VI, we show that our method is also applicable to a class of saddle-focus oscillators that are connected through their linear components. Section VII contains the concluding remarks. The Appendix details the application of the method to a network of a piecewise linear saddle-focus oscillator.

II. THE MULTILAYER NETWORK MODEL

We first consider a two-layer undirected network of N Rössler oscillators

$$\dot{x}_{i} = -y_{i} - z_{i} + \varepsilon_{x} \sum_{j=1}^{N} d_{ij}(x_{j} - x_{i}),
\dot{y}_{i} = x_{i} + ay_{i} + \varepsilon_{y} \sum_{j=1}^{N} g_{ij}(y_{j} - y_{i}),
\dot{z}_{i} = b + (x_{i} - c)z_{i}, \quad i = 1, \dots, N,$$
(1)

where a = 0.2, b = 0.2, and c = 9 are the standard parameter values that yield chaotic behavior of uncoupled Rössler oscillators. $D = (d_{ii})$ and $G = (g_{ii})$ are $N \times N$ symmetric adjacency matrices which correspond to the x and y coupling layers, and nonzero $d_{ij} = 1$ and $g_{ij} = 1$ define links in the two layers. ε_x and ε_y are coupling strengths. Complete synchronization in network (1) is defined by the synchronization manifold $S = \{\mathbf{x}_1(t) = \mathbf{x}_2(t) = \cdots = \mathbf{x}_N(t) = \mathbf{s}(t)\},$ where $\mathbf{x}_i = (x_i, y_i, z_i)$, and the synchronous solution $\mathbf{s}(t) =$ (x(t), y(t), z(t)) is governed by the uncoupled Rössler oscillator. Our main objective is to determine how the interaction of the two-layer couplings affects the stability of synchronization. Note that the x coupling induces synchronization of the bounded type in single-layer networks of Rössler oscillators [20], whereas the y coupling yields the unbounded-type behavior (Fig. 1).

III. A PUZZLE: THE ROLE-EXCHANGE EFFECT

To illustrate the complexity of assessing multilayer connections in inducing or hindering the synchronization even in small networks, we consider the simplest three-node mul-

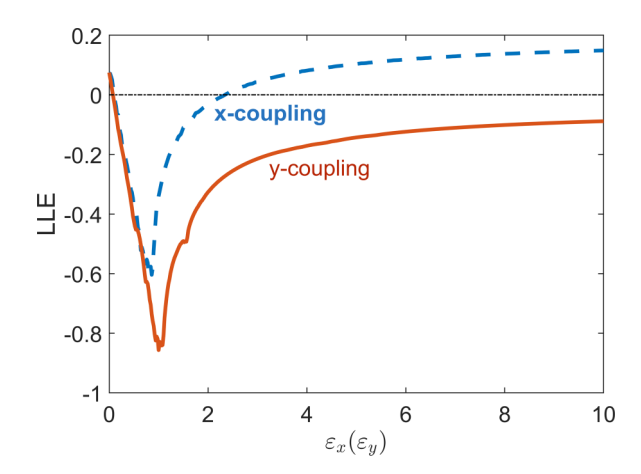


FIG. 1. Largest Lyapunov exponent (LLE) for the stability of synchronization in the single layer two-node network of Rössler oscillators as a function of coupling strength ε_x (ε_y). Dashed blue line shows a bonded interval of coupling ε_x for stable synchronization of x-coupled oscillators. Red solid line shows an unbounded interval of coupling ε_y for stable synchronization of y-coupled oscillators.

tilayer network (1) with one x link $d_{12} = 1$ and one y link $g_{23} = 1$, as depicted in Fig. 2. Remarkably, two striking effects appear. First, the x coupling switches its type from bounded to unbounded and supports stable synchronization for any sufficiently large values of ε_x , provided that ε_y is in some range of intermediate coupling strength (see the dark region in Fig. 2). Second, the y coupling switches its synchronizing role from unbounded to bounded and destabilizes synchronization for sufficiently large values of ε_y , provided

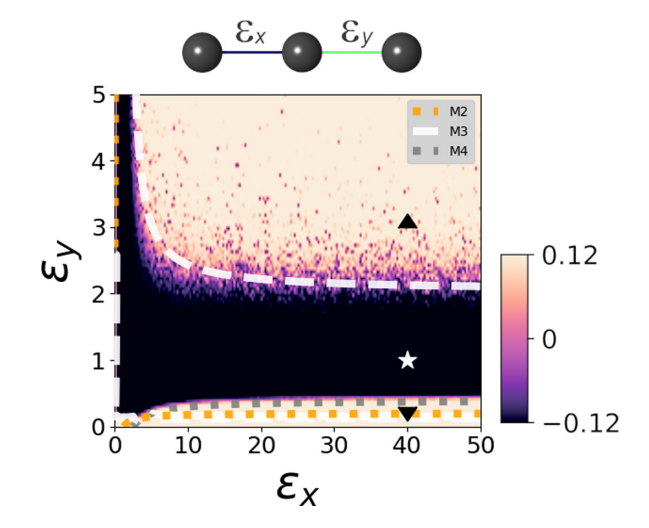


FIG. 2. (top) Three-node multilayer network (1). (bottom) Stability of synchronization as a function of x and y layer coupling strengths, ε_x and ε_y . Color-coding corresponds to values of the largest transverse Lyapunov exponent, numerically calculated via (2). Dark color indicates stability, while light color depicts instability. Yellow short-dashed, white long-dashed, gray short-dashed lines are analytical curves $M_2 = 0$, $M_3 = 0$, and $M_4 = 0$, respectively. Analytical curve $M_1 = 0$ yields the condition that is guaranteed by the other curves and therefore is not shown. Sample points Δ , \star , and ∇ correspond to the plots in Fig. 3.

that ε_x is sufficiently large. This puzzle calls for an explanation and ultimately motivates the development of an effective approach that can predict the stability bounds at which the layers reverse their synchronizing and desynchronizing roles.

Following the standard stability approach [20], we linearize three-node system (1) around synchronous solution $\mathbf{s}(t)$ and obtain the variational stability equations

$$\dot{\xi}_{12} = -\eta_{12} - \zeta_{12} - 2\varepsilon_{x}\xi_{12}, \quad \dot{\eta}_{12} = \xi_{12} + a\eta_{12} + \varepsilon_{y}\eta_{23},
\dot{\zeta}_{12} = z(t)\xi_{12} + [x(t) - c]\zeta_{12}, \quad \dot{\xi}_{23} = -\eta_{23} - \zeta_{23} + \varepsilon_{x}\xi_{12},
\dot{\eta}_{23} = \xi_{23} + a\eta_{23} - 2\varepsilon_{y}\eta_{23}, \quad \dot{\zeta}_{23} = z(t)\xi_{23} + [x(t) - c]\zeta_{23},
(2)$$

where $\xi_{ij} = x_i - x_j$, $\eta_{ij} = y_i - y_j$, and $\zeta_{ij} = z_i - z_j$, i = 1, j = 2 and i = 2, j = 3 are transverse perturbations.

Note that the connectivity matrices for the *x* and *y* layers of this simplest two-layer network do not commute. Therefore, the master stability function [20] cannot be applied to diagonalize and decouple system (2) into two three-dimensional (3D) systems whose stability would be controlled by the eigenvalues of the connectivity matrices. Technically, the simultaneous block-diagonalization [10] can handle this case of the noncommuting matrices; unfortunately, its application transforms the six-dimensional (6D) system (2) into a more complex 6D system¹ without reducing its dimensionality. Therefore, one has to rely on numerical simulations of the full 6D system that offer little insight into the underpinnings of the role-exchanging effect.

Instead, we propose to constructively exploit structural intrinsic properties of the Rössler oscillator to simplify and transform stability equation (2) into an analytically tractable, predictive tool. The synchronous trajectory $\mathbf{s}(t)$ is governed by the Rössler system which exhibits chaotic dynamics centered around a saddle-focus at the origin. The origin is unstable in the xy plane, which corresponds to the unstable focus part while the z direction indicates the one-dimensional (1D) stable manifold of the saddle-focus [43]. The synchronous trajectory is an outward spiral which spends most of the time on or close to the xy plane and then makes a large excursion along the vertical z direction to return back to the xy plane (Fig. 3). This important property suggests that the overall transverse stability of the synchronous trajectory is essentially controlled by the focal part of the synchronous trajectory that lies in the xy plane. Our numerical calculations of the instantaneous Lyapunov exponent corresponding to the transverse stability of the synchronous solution confirm this claim and indicate that synchronization becomes stable as long as the instantaneous transverse Lyapunov exponent becomes negative along the focal part of s (Fig. 3). Therefore, stability equation (2) can be reduced to the linear system with constant

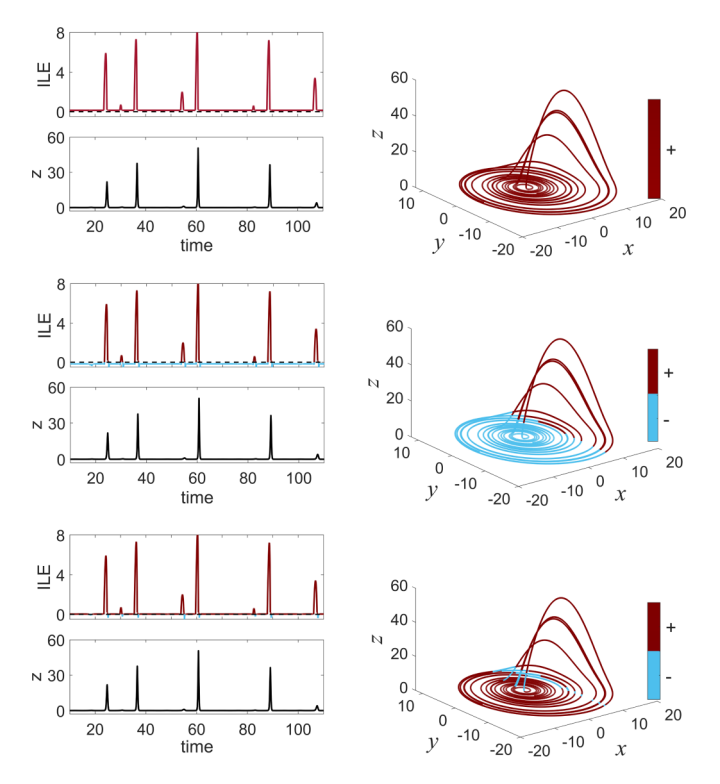


FIG. 3. (left column) Instantaneous Lyapunov exponent (ILE) for the stability of synchronization and the z time series for the parameters corresponding to points Δ , \star , and ∇ in Fig. 2 from top to bottom, respectively. (right column) The synchronous trajectory $\mathbf{s} = (x, y, z)$ whose red (blue) part corresponds to a positive (negative) instantaneous Lyapunov exponent. Note that the transverse stability of the focal part of the trajectory in the (x, y) plane determines the overall stability of synchronization (middle row panel).

coefficients

$$\dot{\xi}_{12} = -\eta_{12} - 2\varepsilon_x \xi_{12}, \quad \dot{\eta}_{12} = \xi_{12} + a\eta_{12} + \varepsilon_y \eta_{23},
\dot{\xi}_{23} = -\eta_{23} + \varepsilon_x \xi_{12}, \quad \dot{\eta}_{23} = \xi_{23} + a\eta_{23} - 2\varepsilon_y \eta_{23},$$
(3)

by ignoring the ζ_{ij} perturbations corresponding to nonzero values of z(t). The stability of linear system (3) yields stable synchronization and can be assessed via the characteristic equation

$$\lambda^4 + \alpha_1 \lambda^3 + \alpha_2 \lambda^2 + \alpha_3 \lambda + \alpha_4 = 0, \tag{4}$$

where $\alpha_1 = 2(\varepsilon_x + \varepsilon_y - a)$, $\alpha_2 = a^2 - 4a\varepsilon_x - 2a\varepsilon_y + 4\varepsilon_x\varepsilon_y + 2$, $\alpha_3 = 2(a^2\varepsilon_x - 2a\varepsilon_x\varepsilon_y - a + \varepsilon_x + \varepsilon_y)$, $\alpha_4 = -2a\varepsilon_x + \varepsilon_x\varepsilon_y + 1$. By the Routh-Hurwitz stability criterion, all eigenvalues λ have negative real parts if the principal diagonal minors of the Hurwitz matrix are positive so that $M_1 = \alpha_1 > 0$, $M_2 = \alpha_1\alpha_2 - \alpha_3 > 0$, $M_3 = \alpha_1\alpha_2\alpha_3 - a_1^2a_4 - a_0a_3^2 > 0$, $M_4 = \alpha_4 > 0$. Figure 2 shows that analytical stability bounds $M_1, M_2, M_3, M_4 = 0$ coincide with the actual bounds to a high degree allowed by the constraints and imperfections imposed by numerical simulations. More specifically, the lower border of the stability region (dark) in Fig. 2 is predicted by the curve $\varepsilon_y = 2a - 1/\varepsilon_x$ that follows from $M_4 = 0$. The upper border of the stability region in Fig. 2 is bounded by the upper curve governed by the condition $M_3 = 0$ and defined by implicit

¹The simultaneous block diagonalization transforms variational equations (2) into the 6D coupled system $\dot{\xi}_{12} = -\eta_{12} - \zeta_{12} - 2\varepsilon_x \xi_{12}$, $\dot{\eta}_{12} = \xi_{12} + a\eta_{12} + \varepsilon_y (\frac{\sqrt{3}}{2}\eta_{23} - \frac{1}{2}\eta_{12})$, $\dot{\zeta}_{12} = z(t)\xi_{12} + (x(t) - c)\zeta_{12}$, $\dot{\xi}_{23} = -\eta_{23} - \zeta_{23}$, $\dot{\eta}_{23} = \xi_{23} + a\eta_{23} + \varepsilon_y (\frac{\sqrt{3}}{2}\eta_{12} - \frac{3}{2}\eta_{23})$, $\dot{\zeta}_{23} = z(t)\xi_{23} + (x(t) - c)\zeta_{23}$.

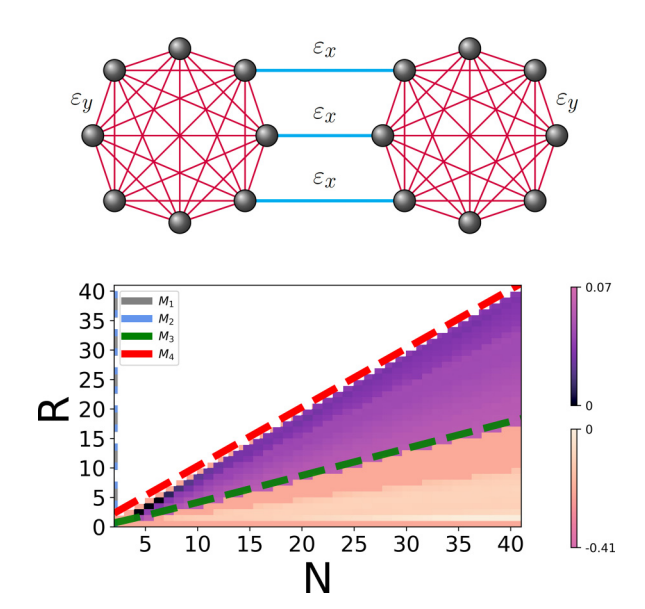


FIG. 4. (top) Two-layer network of 2N oscillators. The layers with global intralayer y coupling are connected via R interlayer x links. (bottom) Stability of synchronization as a function of layer size N and number of interlayer links R. Purple (tan) region corresponds to negative (positive) largest transverse Lyapunov exponent, numerically calculated via the 6D two-node mode system. White region corresponds to irrelevant values of R > N and should be ignored. Color dashed lines are analytical curves $M_1, M_2, M_3, M_4 = 0$. Analytical curve $M_3 = 0$ precisely predicts the loss of stability with increasing N for a fixed R. Parameters $\varepsilon_x = 1$ and $\varepsilon_y = 1$.

function $f(\varepsilon_x, \varepsilon_y) = 0.2$ Considered together, these analytical curves effectively predict the role-exchange effect of the x and y coupling in stabilizing and destabilizing synchronization and resolve the puzzle.

IV. LARGE NETWORKS ALLOWING SIGNIFICANT SIMULTANEOUS BLOCK DIAGONALIZATION REDUCTION

Figure 4 shows a well-known example of a two-layer 2N-node network which consists of two fully y-connected subnetworks with N nodes within each subnetwork and R x links between the subnetworks [10]. It was previously shown that the variational equations for the stability of synchronization manifold S in this network can be reduced via SBD to a two-node transverse mode and (2N-3) one-node transverse modes where the latter are represented by two distinct sets of identical systems [10]. For the network of Rössler oscillators (1), the variational equations for the two-node transverse mode can take the form

$$\begin{split} \dot{\xi}_1 &= -\eta_1 - \zeta_1 - 2\varepsilon_x \xi_1, \\ \dot{\eta}_1 &= \xi_1 + a\eta_1 - (N - R)\varepsilon_y \eta_1 + \gamma \varepsilon_y \eta_2, \\ \dot{\zeta}_1 &= z(t)\xi_1 + [x(t) - c]\zeta_1, \end{split}$$

$$\begin{array}{c} {}^2f(\varepsilon_x,\varepsilon_y)=a^5\varepsilon_x-4a^4\varepsilon_x^2-5a^4\varepsilon_x\varepsilon_y-a^4+4a^3\varepsilon_x^3+16a^3\varepsilon_x^2\varepsilon_y+\\ 8a^3\varepsilon_x\varepsilon_y^2+4a^3\varepsilon_x+4a^3\varepsilon_y-12a^2\varepsilon_x^3\varepsilon_y-20a^2\varepsilon_x^2\varepsilon_y^2-5a^2\varepsilon_x^2-\\ 4a^2\varepsilon_x\varepsilon_y^3-13a^2\varepsilon_x\varepsilon_y-5a^2\varepsilon_y^2+8a\varepsilon_x^3\varepsilon_y^2+2a\varepsilon_x^3+8a\varepsilon_x^2\varepsilon_y^3+\\ 12a\varepsilon_x^2\varepsilon_y+12a\varepsilon_x\varepsilon_y^2+2a\varepsilon_y^3-3\varepsilon_x^3\varepsilon_y-6\varepsilon_x^2\varepsilon_y^2-3\varepsilon_x\varepsilon_y^3=0. \end{array}$$

$$\dot{\xi}_2 = -\eta_2 - \zeta_2,
\dot{\eta}_2 = \xi_2 + a\eta_2 - R\varepsilon_y \eta_2 + \gamma \varepsilon_y \eta_1,
\dot{\zeta}_2 = z(t)\xi_2 + [x(t) - c]\zeta_2,$$
(5)

where $\gamma = \sqrt{(N-R)R}$, and (ξ_1, η_1, ζ_1) and (ξ_2, η_2, ζ_2) are transverse perturbations associated with eigen-like modes 1 and 2. The variational equations for 2N - 2 - R identical one-node transverse modes (ξ_l, η_l, ζ_l) and R-1 identical one-node transverse modes (ξ_k, η_k, ζ_k) are given below.^{3,4} To derive the variational equations, we used a SBD algorithm [45] that yielded an outcome different from that of Ref. [10]; however, the stability argument is essentially the same. While the dimensionality reduction from the 2N-node network is significant, to assess the stability of synchronization, one has to numerically analyze the 6D variational system for the two-node mode system (5) and two 3D systems for each one-mode system. As a result, the origins of emergent stability and instability of synchronization as a function of intra- and interlayer connections and the network size remain difficult to identify.

To resolve this problem, we apply our approximation method by removing the ζ_1 and ζ_2 variables and equations from system (5) and therefore turning (5) into a four-dimensional (4D) linear system. The stability of this 4D linear system with constant coefficients can be determined through the characteristic equation (A6) with new coefficients $\alpha_1 = N\varepsilon_y + 2\varepsilon_x - 2/5$, $\alpha_2 = 2N\varepsilon_x\varepsilon_y - N\varepsilon_y/5 - 4\varepsilon_x/5 + 51/25$, $\alpha_3 = -\frac{2N\varepsilon_x\varepsilon_y}{5} + N\varepsilon_y + \frac{52\varepsilon_x}{25} - \frac{2}{5}$, and $\alpha_4 = \frac{1}{2}$ $2N\varepsilon_x\varepsilon_y - 2R\varepsilon_x\varepsilon_y - \frac{2\varepsilon_x}{5} + 1$. Bounds for the stability of the 4D linear system determined by minors $M_1, M_2, M_3, M_4 = 0$ of the corresponding Hurwitz matrix are plotted in Fig. 4. Notice that analytical bound $M_3 = 0$ (green dashed line) coincides with the actual bound for the stability of synchronization in the two-layer network, revealed through numerical simulations of 6D variational system (5). The stability bounds for one-node modes (ξ_l, η_l, ζ_l) and (ξ_k, η_k, ζ_k) lie within the stability region of the 4D linear system and therefore are not shown. The white region in Fig. 4 corresponds to the two-layer network with R > N which has a distinct network structure with at least one node having more than one interlayer link, and therefore, requiring a separate SBD reduction different from (5). Remarkably, our study analytically predicts a surprising effect that increasing the size of the globally coupled layer, N, which in isolation would promote synchronization, makes the two-layer network unsynchronizable (note the loss of stability with increasing N for a fixed R in Fig. 4).

V. ARBITRARY NETWORK TOPOLOGIES

As our method turns the variational equations into a linear system, the stability of synchronization can be treated in terms of the eigenvalues of the $2(N-1) \times 2(N-1)$ matrix M associated with the corresponding reduced variational equations.

 $^{{}^{3,}\}dot{\xi}_{l} = -\eta_{l} - \zeta_{l}, \ \dot{\eta}_{l} = \xi_{l} + a\eta_{1} - NR\varepsilon_{y}\eta_{l}, \ \dot{\zeta}_{l} = z(t)\xi_{l} + [x(t) - c]\zeta_{l},$ $l = 3, \dots, 2N - R.$

 $^{{}^{4}\}dot{\xi}_{k} = -\eta_{k} - \zeta_{k} - 2\varepsilon_{x}\xi_{k}, \ \dot{\eta}_{k} = \xi_{k} + a\eta_{1} - NR\varepsilon_{y}\eta_{k}, \ \dot{\zeta}_{k} = z(t)\xi_{k} + [x(t) - c]\zeta_{k}, k = 2N - R + 1, \dots, 2N - 1.$

Therefore, our method can reliably predict stable synchronization in complex multilayer networks (1) for which the SBD may not yield any meaningful reduction. More specifically, the variational equations for transverse stability of synchronization in two-layer networks of *N* Rössler oscillators (1) with an arbitrary network structure can be cast into the form

$$\dot{\xi}_{ij} = -\eta_{ij} - \zeta_{ij} + \varepsilon_x \sum_{k=1}^{N} (d_{jk}\xi_{jk} - d_{ik}\xi_{ik}),
\dot{\eta}_{ij} = \xi_{ij} + a\eta_{ij} + \varepsilon_y \sum_{k=1}^{N} (g_{jk}\eta_{jk} - g_{ik}\eta_{ik}),
\dot{\zeta}_{ij} = z(t)\xi_{ij} + [x(t) - c]\zeta_{ij},$$
(6)

where $\xi_{ij} = x_i - x_j$, $\eta_{ij} = y_i - y_j$, and $\zeta_{ij} = z_i - z_j$, i = 1, ..., N-1, j = i+1 are N-1 linearly independent transverse perturbations.

Removing the ζ_{ij} variables and equations and therefore ignoring the dynamics of perturbations away from the focal part of synchronous solution $\mathbf{s}(t)$, we reduce $3(N-1) \times 3(N-1)$ variational equations (6) with time-dependent coefficients driven by z(t) and x(t) to the following linear differential equations:

$$\dot{\xi}_{ij} = -\eta_{ij} - \zeta_{ij} + \varepsilon_x \sum_{k=1}^{N} (d_{jk}\xi_{jk} - d_{ik}\xi_{ik}),$$

$$\dot{\eta}_{ij} = \xi_{ij} + a\eta_{ij} + \varepsilon_y \sum_{k=1}^{N} (g_{jk}\eta_{jk} - g_{ik}\eta_{ik}),$$
(7)

where $i=1,\ldots,N-1$ and j=i+1. The stability of linear system (7) is determined by the eigenvalues of the corresponding $2(N-1)\times 2(N-1)$ matrix M. While deriving closed form conditions for the negativeness of all $2\times (N-1)$ eigenvalues is out of reach, calculating the largest (least negative) eigenvalue of a $2(N-1)\times 2(N-1)$ matrix in lieu of the largest Lyapunov exponent of a 3(N-1)-dimensional system of variational equations gives a significant computational advantage.

We use a 20-node network composed of two Erdős-Rényi random y-coupled subnetworks connected via random x links (Fig. 5) as an example that does not allow a meaningful SBD reduction. The two-component structure of this network was chosen to preserve the role-exchange effect which might not be present in more homogeneous networks that have both x and y links between their components. Trivial calculations of 2×19 eigenvalues of the corresponding matrix M yield the bound at which the largest eigenvalue of matrix M becomes zero and therefore determines the stability bound for synchronization rather precisely (white dashed line in Fig. 5). The code for setting up matrix M for an arbitrary two-layer network and generating the bounds of Fig. 5 is available [46].

VI. BEYOND RÖSSLER OSCILLATORS

Our method is also applicable to a class of saddle-focus oscillatory systems that, similarly to Rössler oscillator, (i) have linear or piecewise-smooth linear right-hand sides that

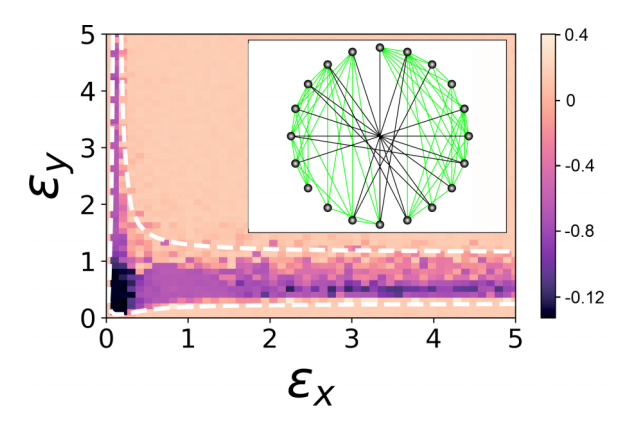


FIG. 5. (inset) Two Erdős-Rényi random subnetworks connected via random links. Links within each subnetwork correspond to y coupling with strength ε_y (light green). Links between the subnetworks are x coupling with ε_x (black). Probability of a y link, $p_y = 0.3$. Probability of an x connection between the first (second) and second (first) halves of the subnetworks is $p_x = 0.6$ ($p_x = 0.24$). (main) Largest transverse Lyapunov exponent for the stability of synchronization in network (1) (heat map). The bound (dashed white lines), at which the largest eigenvalue of matrix M becomes zero, predicts the stability region (black and purple color) remarkably well.

correspond to a focus manifold and (ii) are connected into a network via these linear components. To support this claim, we studied a three-node multilayer network composed of chaotic saddle-focus piecewise-smooth systems [44] that satisfy properties (i) and (ii). Our analysis (detailed in the Appendix) precisely predicted the stability boundaries and indicated that this network has synchronization properties practically identical to those of the Rössler oscillator network, thereby confirming the generic property of the role-exchange effect and broader applicability of the method. Other examples of saddle-focus oscillators that could be treated by the method include Lurie control systems with a nonlinearity in only one of their dynamical equations [47] and Chua circuits [48]. In such systems, it is common practice to implement negative feedback control by connecting the units via their linear components [49,50].

VII. CONCLUSIONS

In this paper, we developed an effective method for assessing the stability of synchronization in multilayer networks of saddle-focus oscillators. It enhances the predictive power of the existing SBD methods [10,15] for networks that allow significant SBD reduction and becomes the ultimate alternative to full-scale simulation of the Lyapunov exponents for arbitrary complex networks for which the SBD reduction is insignificant. The application of this method analytically predicted counterintuitive effects caused by multilayer coupling. In particular, the application of this method reveals and analytically predicts a surprising "role-exchange" effect in which one layer coupling that would destabilize synchronization in a single layer network reverses its role in a two-layer

Beyond the class of saddle-focus oscillators with linear components amenable to analytical treatment, our preliminary analysis indicates that the role-exchange effect is common among other oscillators, including multilayer networks of tritrophic Rozenzweig-MacArthur models coupled via consumer and predator dispersal [39].

Our method also opens the door to applying the master stability function to approximate synchronization in multilayer networks in the presence of small parameter mismatch [25,31,51,52]. This can be done by simply calculating the eigenvalues of the constant matrix corresponding to the slightly mismatched variational equations. Similarly, our approach exploiting the structural intrinsic oscillator properties can enable analytical stability treatment of cluster synchronization [13,53] and synchronization in simplicial complexes [54] by replacing multidimensional variational stability equations with their linear algebraic counterparts.

ACKNOWLEDGMENTS

This work was supported by the National Science Foundation of China under Grants No. 62076104 and No. 11871231 (to L.T.), the National Science Foundation (USA) under Grants No. DMS-1909924 and No. CMMI-2009329 (to K.S, K.D., and I.B.), and the Georgia State University Brains and Behavior Program (to K.S.).

APPENDIX

In this Appendix, we provide evidence that our method can be applied to networks of piecewise linear saddle-focus oscillators with a bounded synchronization region (the bounded type). Similarly to networks of Rössler oscillators (1), we consider the following two-layer network of *N* piecewise linear oscillators:

$$\dot{\mathbf{x}}_i = A_i(\mathbf{x}_i - B_i) + \varepsilon_x \sum_{j=1}^N d_{ij} H_x(\mathbf{x}_j - \mathbf{x}_i)$$

$$+ \varepsilon_y \sum_{j=1}^N g_{ij} H_y(\mathbf{x}_j - \mathbf{x}_i), \tag{A1}$$

where $\mathbf{x}_i = (x_i, y_i, z_i)$, and $A_i = A_0$ and $B_i = B_0$ if $y_i + z_i < 1$; otherwise, $A_i = A_1$ and $B_i = B_1$. Here, $B_0 = 0$, $B_1 = [0, 0.5, 0.5]^{\top}$, and

$$A_0 = \begin{pmatrix} 0.2 & -1 & 0 \\ 1 & 0.2 & 0 \\ 0 & 0 & -2 \end{pmatrix}, \quad A_1 = \begin{pmatrix} -1.5 & 0 & 0 \\ 0 & 0 & -1 \\ 0 & 1 & 0 \end{pmatrix}.$$

 $H_x = \text{diag}\{1, 0, 0\}$ and $H_y = \text{diag}\{0, 1, 0\}$ are inner coupling matrices that yield x and y coupling, respectively. Other notations are as in network (1). The individual unit of the network is a 3D piecewise linear system

$$\dot{\mathbf{x}} = \begin{cases} A_0(\mathbf{x} - B_0), & y + z < 1 \\ A_1(\mathbf{x} - B_1), & y + z \geqslant 1 \end{cases}$$
 (A2)

that was previously shown to exhibit saddle-focus chaos [44]. Figure 6 (right panel) shows its typical chaotic attractor. Figure 7 demonstrates that such piecewise linear oscillators have synchronization properties nearly identical to Rössler oscillators. More precisely, the *x* coupling (*y* coupling) in the

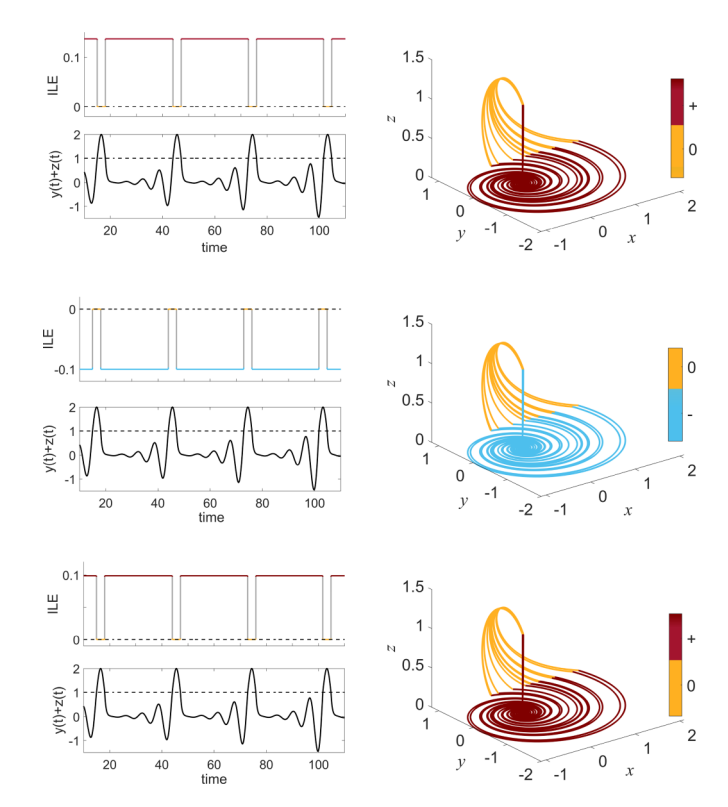


FIG. 6. Diagrams similar to Fig. 3 calculated for the three-node two-layer network of two piecewise linear oscillators (A2). (left column) Instantaneous Lyapunov exponent (ILE) for the stability of synchronization and the y+z time series for the parameters corresponding to points Δ , \star , and ∇ in Fig. 8 from top to bottom, respectively. (right column) The synchronous trajectory $\mathbf{s} = (x, y, z)$ whose red (blue) part corresponds to a positive (negative) instantaneous Lyapunov exponent. Note that the transverse stability of the focal part of the trajectory for y+z<1 plane determines the overall stability of synchronization (middle row panel).

simplest single-layer two-node network (A1) yields a bounded (unbounded) interval of synchronization.

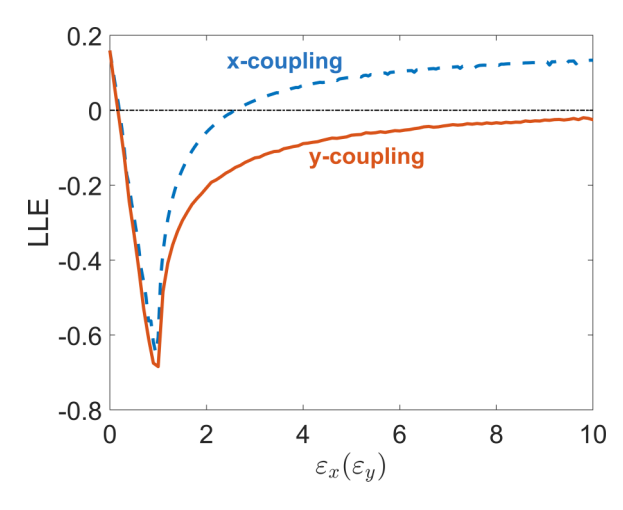


FIG. 7. Master stability function for synchronization of two piecewise linear oscillators (A2). Note the striking resemblance with the master stability function for Rössler oscillators in Fig. 1.

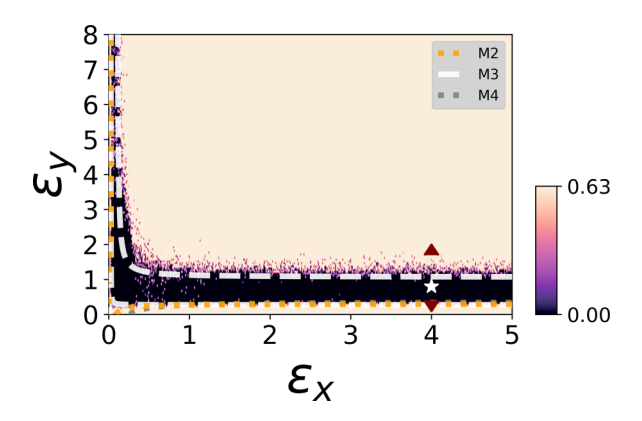


FIG. 8. Stability diagram similar to Fig. 2 but calculated for the three-node two-layer network of two piecewise linear oscillators (A2). Color coding corresponds to the synchronization error averaged over the last 1000 integration steps. Dark color indicates stability, while light color depicts instability. Yellow short-dashed, white long-dashed, gray short-dashed lines are analytical curves $M_2 = 0$, $M_3 = 0$, and $M_4 = 0$, respectively. As in Fig. 2, analytical curve $M_1 = 0$ yields the condition that is guaranteed by the other curves and therefore is not shown. Sample points Δ ($\varepsilon_x = 4$, $\varepsilon_y = 2$), \star ($\varepsilon_x = 4$, $\varepsilon_y = 0.8$), and ∇ ($\varepsilon_x = 4$, $\varepsilon_y = 0.1$) correspond to the plots in Fig. 6.

Figure 8 provides evidence that (i) the role-exchange effect of multilayer connections is also present in the three-node two layer network of piecewise linear oscillators (A2) and (ii) analytical bounds for stable synchronization can be derived similarly to the three-node network of Rössler oscillators in Fig. 2. In this case, we prefer to write the variational equations in the vector form:

$$\dot{\mathbf{x}}_{12} = Df(\mathbf{s})\mathbf{x}_{12} - 2\varepsilon_x H_x \mathbf{x}_{12} + \varepsilon_y H_y \mathbf{x}_{23},
\dot{\mathbf{x}}_{23} = Df(\mathbf{s})\mathbf{x}_{23} + \varepsilon_x H_x \mathbf{x}_{12} - 2\varepsilon_y H_y \mathbf{x}_{23},$$
(A3)

where $\mathbf{x}_{ij} = \mathbf{x}_i - \mathbf{x}_j = (\xi_{ij}, \eta_{ij}, \zeta_{ij})^{\top}$, and $Df(\mathbf{s}) = A_0$ if y + z < 1, otherwise $Df(\mathbf{s}) = A_1$. Exactly as for the Rössler oscillators, our numerical calculations of instantaneous largest transverse Lyapunov exponent indicate that the overall transverse stability of the synchronous trajectory is fully controlled by the focal part of the synchronous trajectory that lies in the region where y + z < 1 and the system dynamics is governed by matrix A_0 (Fig. 6). Therefore, we can turn the variational equations (A3) with coefficients switching between A_0 and A_1 to the following linear variational equations determined via matrix A_0 :

$$\dot{\xi}_{12} = (0.2 - 2\varepsilon_x)\xi_{12} - \eta_{12}, \quad \dot{\eta}_{12} = \xi_{12} + 0.2\eta_{12} + \varepsilon_y\eta_{23},
\dot{\zeta}_{12} = -2\zeta_{12}, \quad \dot{\xi}_{23} = \varepsilon_x\xi_{12} + 0.2\xi_{23} - \eta_{23},
\dot{\eta}_{23} = \xi_{23} + (0.2 - 2\varepsilon_y)\eta_{23}, \quad \dot{\zeta}_{23} = -2\zeta_{23}.$$
(A4)

Removing the uncoupled stable ζ_{12} and ζ_{23} equations, we further reduce (A4) to the 4D linear with constant coefficients:

$$\dot{\xi}_{12} = (0.2 - 2\varepsilon_x)\xi_{12} - \eta_{12}, \quad \dot{\eta}_{12} = \xi_{12} + 0.2\eta_{12} + \varepsilon_y\eta_{23},
\dot{\xi}_{23} = \varepsilon_x\xi_{12} + a\xi_{23} - \eta_{23}, \quad \dot{\eta}_{23} = \xi_{23} + (0.2 - 2\varepsilon_y)\eta_{23}.$$
(A5)

As in the Rössler oscillator case, the stability of linear system (A5) yields stable synchronization and can be assessed via the characteristic equation

$$\lambda^4 + \alpha_1 \lambda^3 + \alpha_2 \lambda^2 + \alpha_3 \lambda + \alpha_4 = 0, \tag{A6}$$

where $\alpha_1 = 2(\varepsilon_x + \varepsilon_y - 2a)$, $\alpha_2 = 6a^2 + 2 - 6a(\varepsilon_x + \varepsilon_y) + 4\varepsilon_x\varepsilon_y$, $\alpha_3 = 2[-2a(a^2 + 1) + (3a^2 + 1)(\varepsilon_x + \varepsilon_y) - 4a\varepsilon_x\varepsilon_y]$, $\alpha_4 = (a^2 + 1)^2 - 2a(a^2 + 1)(\varepsilon_x + \varepsilon_y) + (4a^2 + 1)\varepsilon_x\varepsilon_y$.

Analytical stability bounds $M_1, M_2, M_3, M_4 = 0$ for the principal diagonal minors of the Hurwitz matrix, $M_1 = \alpha_1$, $M_2 = \alpha_1\alpha_2 - \alpha_3$, $M_3 = \alpha_1\alpha_2\alpha_3 - a_1^2a_4 - a_0a_3^2$, and $M_4 = \alpha_4$ are depicted in Fig. 8.

M. Kivelä, A. Arenas, M. Barthelemy, J. P. Gleeson, Y. Moreno, and M. A. Porter, J. Complex Netw. 2, 203 (2014).

^[2] S. V. Buldyrev, R. Parshani, G. Paul, H. E. Stanley, and S. Havlin, Nature (London) 464, 1025 (2010).

^[3] M. De Domenico, C. Granell, M. A. Porter, and A. Arenas, Nat. Phys. 12, 901 (2016).

^[4] N. Kopell and B. Ermentrout, Proc. Natl. Acad. Sci. USA 101, 15482 (2004).

^[5] I. Belykh, R. Reimbayev, and K. Zhao, Phys. Rev. E 91, 062919 (2015).

^[6] S. Boccaletti, G. Bianconi, R. Criado, C. I. Del Genio, J. Gómez-Gardenes, M. Romance, I. Sendina-Nadal, Z. Wang, and M. Zanin, Phys. Rep. 544, 1 (2014).

^[7] D. Taylor, S. Shai, N. Stanley, and P. J. Mucha, Phys. Rev. Lett. 116, 228301 (2016).

^[8] F. Radicchi and G. Bianconi, Phys. Rev. X 7, 011013 (2017).

^[9] F. Sorrentino, New J. Phys. 14, 033035 (2012).

^[10] D. Irving and F. Sorrentino, Phys. Rev. E 86, 056102 (2012).

^[11] C. I. del Genio, J. Gómez-Gardeñes, I. Bonamassa, and S. Boccaletti, Sci. Adv. 2, e1601679 (2016).

^[12] I. Belykh, D. Carter, and R. Jeter, J. Appl. Dyn. Syst. 18, 2267 (2019).

^[13] K. A. Blaha, K. Huang, F. Della Rossa, L. Pecora, M. Hossein-Zadeh, and F. Sorrentino, Phys. Rev. Lett. 122, 014101 (2019).

^[14] F. Della Rossa, L. Pecora, K. Blaha, A. Shirin, I. Klickstein, and F. Sorrentino, Nat. Commun. 11, 3179 (2020).

^[15] Y. Zhang and A. E. Motter, SIAM Rev. 62, 817 (2020).

^[16] X. Zhang, S. Boccaletti, S. Guan, and Z. Liu, Phys. Rev. Lett. 114, 038701 (2015).

^[17] I. Leyva, R. Sevilla-Escoboza, I. Sendiña-Nadal, R. Gutiérrez, J. Buldú, and S. Boccaletti, Sci. Rep. 7, 45475 (2017).

^[18] L. Tang, X. Wu, J. Lü, J.-A. Lu, and R. M. D'Souza, Phys. Rev. E **99**, 012304 (2019).

^[19] J. Sawicki, I. Omelchenko, A. Zakharova, and E. Schöll, Phys. Rev. E 98, 062224 (2018).

^[20] L. M. Pecora and T. L. Carroll, Phys. Rev. Lett. 80, 2109 (1998).

^[21] S. Boccaletti, J. Kurths, G. Osipov, D. Valladares, and C. Zhou, Phys. Rep. **366**, 1 (2002).

^[22] M. Barahona and L. M. Pecora, Phys. Rev. Lett. 89, 054101 (2002).

- [23] C. W. Wu, Synchronization in Coupled Chaotic Circuits & Systems (World Scientific, Singapore, 2022), Vol. 41.
- [24] X. F. Wang and G. Chen, IEEE Trans. Circuits Syst. I 49, 54 (2002).
- [25] V. N. Belykh, I. V. Belykh, and M. Hasler, Phys. D (Amsterdam, Neth.) 195, 159 (2004).
- [26] I. Belykh, V. Belykh, and M. Hasler, Phys. D (Amsterdam, Neth.) 224, 42 (2006).
- [27] C. W. Wu, IEEE Trans. Autom. Control 51, 1207 (2006).
- [28] Z. Li and G. Chen, IEEE Trans. Circuits Syst. II: Express Br. 53, 28 (2006).
- [29] I. Belykh, E. de Lange, and M. Hasler, Phys. Rev. Lett. 94, 188101 (2005).
- [30] I. Belykh and A. Shilnikov, Phys. Rev. Lett. 101, 078102 (2008).
- [31] J. Sun, E. M. Bollt, and T. Nishikawa, Europhys. Lett. 85, 60011 (2009).
- [32] T. Nishikawa and A. E. Motter, Proc. Natl. Acad. Sci. USA 107, 10342 (2010).
- [33] J. Aguirre, R. Sevilla-Escoboza, R. Gutiérrez, D. Papo, and J. M. Buldú, Phys. Rev. Lett. 112, 248701 (2014).
- [34] L. Zhang, A. E. Motter, and T. Nishikawa, Phys. Rev. Lett. 118, 174102 (2017).
- [35] T. Nishikawa, J. Sun, and A. E. Motter, Phys. Rev. X 7, 041044 (2017).
- [36] K. Daley, K. Zhao, and I. V. Belykh, Chaos 30, 043102 (2020).
- [37] S. Panahi, N. Amaya, I. Klickstein, G. Novello, and F. Sorrentino, Phys. Rev. E 105, 014313 (2022).
- [38] R. Reimbayev, K. Daley, and I. Belykh, Philos. Trans. R. Soc. A 375, 20160282 (2017).

- [39] I. Belykh, C. Piccardi, and S. Rinaldi, J. Biol. Dyn. 3, 497 (2009).
- [40] A. Stefański, P. Perlikowski, and T. Kapitaniak, Phys. Rev. E **75**, 016210 (2007).
- [41] P. Perlikowski, A. Stefanski, and T. Kapitaniak, Int. J. Non-Linear Mech. 45, 895 (2010).
- [42] S. Boccaletti, V. Latora, Y. Moreno, M. Chavez, and D.-U. Hwang, Phys. Rep. 424, 175 (2006).
- [43] O. E. Rössler, Phys. Lett. A 57, 397 (1976).
- [44] J. G. Barajas-Ramírez, A. Franco-López, and H. G. González-Hernández, Appl. Math. Comput. 395, 125877 (2021).
- [45] K. Murota, Y. Kanno, M. Kojima, and S. Kojima, Jpn. J. Ind. Appl. Math. 27, 125 (2010).
- [46] https://doi.org/10.5281/zenodo.6676588
- [47] V.-M. Popov and R. Georgescu, *Hyperstability of Control Systems* (Springer, Berlin, 1973).
- [48] R. N. Madan, *Chua's Circuit: A Paradigm for Chaos* (World Scientific, Singapore, 1993).
- [49] H. Nijmeijer, Phys. D (Amsterdam, Neth.) 154, 219 (2001).
- [50] G. Chen and X. Yu, Chaos Control: Theory and Applications (Springer Science & Business Media, Heidelberg, 2003), Vol. 292.
- [51] A. E. Hramov, A. E. Khramova, A. A. Koronovskii, and S. Boccaletti, Int. J. Bifurc. Chaos Appl. Sci. Eng. 18, 845 (2008).
- [52] F. Sorrentino and M. Porfiri, Europhys. Lett. 93, 50002 (2011).
- [53] L. M. Pecora, F. Sorrentino, A. M. Hagerstrom, T. E. Murphy, and R. Roy, Nat. Commun. 5, 4079 (2014).
- [54] L. V. Gambuzza, F. Di Patti, L. Gallo, S. Lepri, M. Romance, R. Criado, M. Frasca, V. Latora, and S. Boccaletti, Nat. Commun. 12, 1255 (2021).